Xuegang Li, Linh V. Nguyen, Yong Zhao, Heike Ebendorff-Heidepriem, Stephen C. Warren-Smith

High-sensitivity Sagnac-interferometer biosensor based on exposed core microstructured optical fiber

Sensors and Actuators B: Chemical, 2018; 269:103-109

High-sensitivity Sagnac-interferometer biosensor based on exposed core microstructured optical fiber

Xuegang Li, [1, 2,*] Linh V. Nguyen,[1, 4] Yong Zhao,[2] Heike Ebendorff-Heidepriem[1,3] and Stephen C. Warren-Smith[1,3]

[1]Institute for Photonics and Advanced Sensing (IPAS) and School of Physical Sciences, The University of Adelaide, Adelaide, South Australia 5005, Australia
[2]College of Information Science and Engineering, Northeastern University, Shenyang 110819, China
[3]ARC Centre of Excellence for Nanoscale BioPhotonics (CNBP), The University of Adelaide, Adelaide, South Australia 5005, Australia
[4]Plant Biosecurity Cooperative Research Centre, Bruce, Canberra 2617, ACT, Australia

Abstract—A novel, high sensitivity Sagnac-interferometer biosensor based on exposed core microstructured optical fiber (ECF) has been designed and implemented in this paper. The exposed core fiber has noncircular symmetry and thus exhibits birefringence and can form a sensing element within a Sagnac loop interferometer. The exposed-core fiber design provides direct access to the evanescent field, allowing the measurement of bulk refractive index (RI) with a sensitivity of up to -3,137 nm/RIU while maintaining the fiber's robustness. The sensor can also detect the localized refractive index changes at the fiber core's surface as the result of a biological binding event. We demonstrate the use of this sensor for label-free sensing of biological molecules by immobilizing biotin onto the fiber core as the probe to capture the target molecule streptavidin.

Keywords: biosensor, Sagnac-interferometer, refractive index measurement, exposed-core microstructured optical fiber.

1. Introduction

Bio-sensing is important for many applications in public health research, environmental science, biological engineering, disease diagnosis and pharmaceutical research. Biosensors have been developed based on a wide variety of techniques, including electrochemical conductance [1], use of nanowires/nanotubes [2, 3] , optical ring resonators [4, 5], fluorescence [6-8] and fiber-optic sensors [9-20]. Among them, fiber-optic biosensors have recently been extensively investigated due to their bio-compatibility, small size, high measurement resolution, high stability, ability to operate remotely and in harsh conditions, and immunity to electromagnetic interference. Various methods for creating fiber-optic biosensors have been reported, such as using fiber Bragg-gratings [9-11], long period fiber gratings [12-15], tilted fiber Bragg gratings [16], Fabry–Perot interferometers [17, 18], Mach–Zehnder interferometers [19, 20], micro-fiber Sagnac interferometers [21], and surface plasmon resonance [22-25].

The majority of these biosensors are based on the refractive index (RI) change induced by a molecular binding event on the sensor surface, which is directly related to the sample concentration. Therefore, a primary goal for sensor development is to increase the sensitivity to refractive index changes. Fiber Bragg gratings and long period gratings [9-15] are commonly implemented, but these sensors suffer low sensitivity and complicated device fabrication processes. Likewise, interferometric devices such as Fabry–Perot interferometers (FPIs) [17, 18] and Mach–Zehnder interferometers [19] typically have low refractive index sensitivity without post-processing such as tapering and etching, which can compromise the mechanical strength and the robustness of the fiber. Surface plasmon resonance (SPR) is a technique that boasts high sensitivity, but relies on the use of metal films that suffer instability issues and high loss in an optical fiber configuration [22-25]. An alternative high refractive index sensitivity fiber-optic sensor is based on micro-

fiber Sagnac interferometers, which can reach sensitivities as high as 12,500 nm/RIU [26] and have been demonstrated as effective biosensors [21]. However, they are based on tapered fibers that can easily be damaged due to their thin, micron-scaled, diameters [21, 26].

Exposed-core microstructured optical fibers (ECFs) offer high sensitivity via direct access to the evanescent field, but in a robust configuration that can be practically handled [19]. In this paper we exploit the noncircular symmetry, thus birefringence, of the ECF by implementing it in a Sagnac interferometer for biological sensing. Since the birefringence of ECF is highly sensitive to external materials through the evanescent field of the guided light, the Sagnac interferometer has a higher sensitivity to external RI than the Mach-Zehnder interferometer configuration.

2. Operating principle

2.1 Exposed-core fiber Sagnac interferometer: configuration

Fig. 1 shows a schematic diagram of the proposed Sagnac interferometer based on the ECF. Light from a broad-band source is split into clockwise and counterclockwise beams via a 3 dB coupler as it enters the loop. A net phase difference is accumulated as the two polarization states propagate through the length of the birefringent ECF, leading to interference when the two beams are recombined at the coupler, which is then measured on an optical spectrum analyzer (OSA).

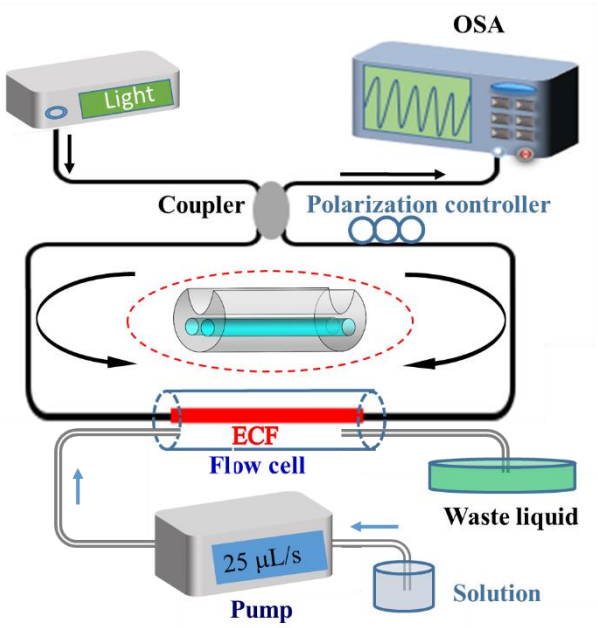

Fig. 1 Schematic diagram of the proposed sensing system.

Ignoring any insertion losses of the Sagnac loop, the transmission ratio of optical intensity injected into the Sagnac interferometer in terms of phase difference can be described as,

$$T=\left[1-\cos\left(\psi\right)\right]/2\,, \tag{1}$$

where $\psi = 2\pi LB(\lambda,n)/\lambda$ is the phase difference, λ is the operating wavelength, and L is the length of the ECF used. $B(\lambda,n)$ is the birefringence of the ECF, which is a function of external RI (n) and wavelength (λ). The interference spectrum minima, λ_{min}, occur when phase matching conditions are satisfied:

$$\frac{2\pi B(\lambda,n)L}{\lambda_{\min}} = 2m\pi\,, \tag{2}$$

where *m* is an integer. Eq. (2) shows how the positions of the interference spectrum minima change with birefringence.

2.2 Birefringence of the exposed-core microstructured optical fiber

Fig. 2 shows a cross-sectional image of the ECF, which is a special type of microstructured optical fiber whose suspended core is exposed to the surrounding medium on one side [27]. The open side causes an asymmetry in the fiber core, which creates a birefringence. This becomes pronounced when the fiber is immersed in a liquid (for example, for sensing), as the refractive index profile becomes particularly asymmetric.

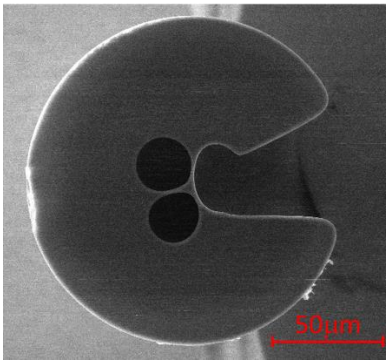

Fig. 2. Scanning electron microscope (SEM) image of the exposed-core microstructured optical fiber.

In order to understand the birefringence properties of the ECF, the structure was investigated using a finite-element method (COMSOL v5.2). Fig. 3 (a) shows the geometry of the fiber used for the simulation, where blue refers to the air, grey refers to the silica glass core and green refers to either air or liquid on the exposed side of the fiber. In this simulation, the exposed side of the ECF has been set as water because this is more relevant to sensing. Fig. 3 (b) and Fig. 3 (c) are the simulated electric field intensity distributions for the x-polarized and y-polarized fundamental modes.

The birefringence *B* can be expressed as follows:

$$B = \left| n_x - n_y \right|, \tag{3}$$

where, n_x and n_y are the effective refractive indices of the x-polarized and y-polarized modes. It can been seen from Fig. 3 (b) and Fig. 3 (c) that there are a phase birefringence of $B = \left| n_x - n_y \right| = 7.42 \times 10^{-5}$ at 1300 nm in the ECF. 1300 nm is the center wavelength in our experiment spectrum. This phase birefringence will thus allow the optical fiber to be used within a Sagnac interferometer configuration as the two polarization modes will lead to two different optical path lengths.

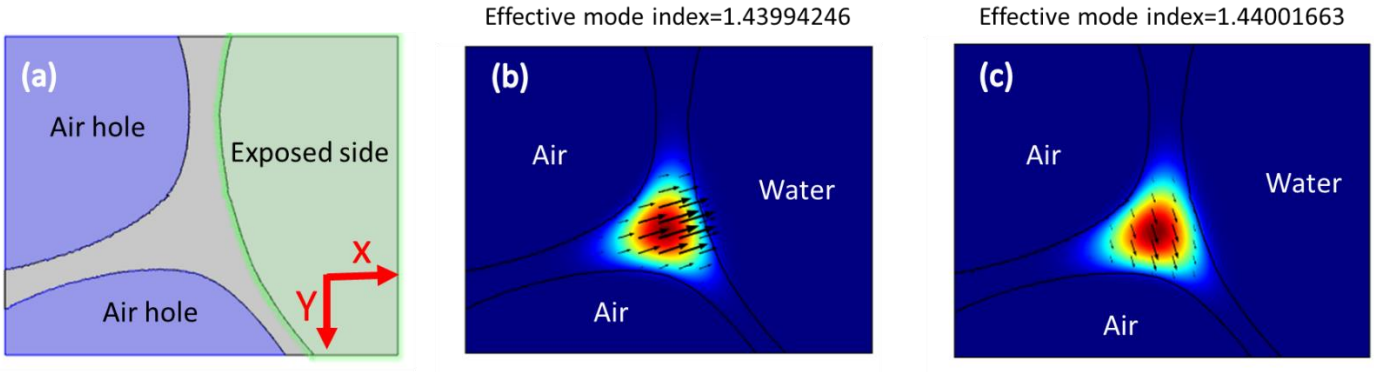

Fig. 3 (a) Geometry of the theoretical model used for simulation, blue is air, grey is silica and green is exposed to the external environment, (b) and (c) are the simulated electric field intensity distributions of the x-polarized and y-polarized fundamental modes, respectively, where the exposed side is water.

2.3 Modelling of RI sensitivity

To determine the potential sensitivity of the ECF to bulk RI when used in a Sagnac interferometer configuration, we varied the refractive index of the sensing-liquid filled in the exposed side of Fig. 3 (a). The birefringence of the ECF when the external refractive index changes is shown in Fig. 4 (a). It can be seen that increasing the refractive index leads to an increase in birefringence. This can be understood by considering that the two polarization modes have different proportions of propagating optical fields in the open core section. They will thus have different relative sensitivities to external refractive index, leading to the shifts of the transmission Sagnac spectra, which was generated by a 20 cm ECF Sagnac interferometer, as shown in Fig. 4 (b). The theoretical bulk RI sensitivity of the sensor is -2,592 nm/RIU.

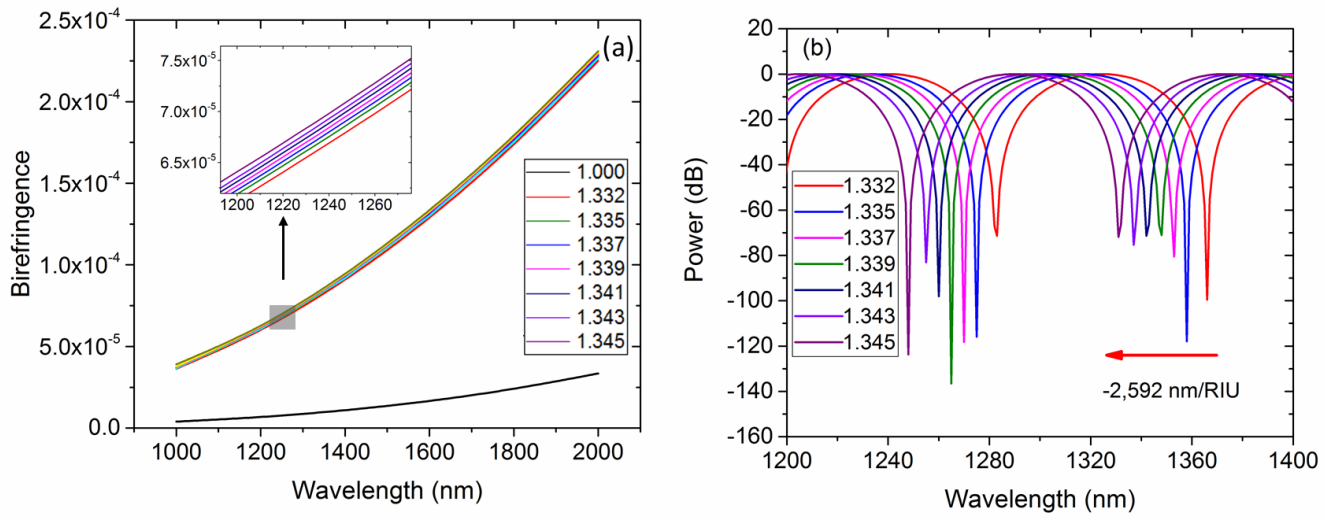

Fig. 4 (a) Phase birefringence, *B*, with different bulk RI dependence on wavelength λ, (b) the simulated transmission Sagnac spectra with different external bulk RI.

2.4 Modelling of thin-film sensitivity

In order to utilize an optical fiber as a selective biosensor, it is necessary that it is sensitive to binding events on the surface, which are effectively thin-films [4, 5, 12, 18, 19]. Therefore, we have investigated theoretically the sensitivity of the ECF birefringence to thin-films using the same analytical method as above but now with a thin-film on the exposed-core. In the simulation, RI of the thin-film was set as 1.54, which corresponds to a polyelectrolyte coating [18]. The results are shown in Fig. 5 (a). For a high RI thin film, with the thickness increasing, the effective indices of the x-polarization and y-polarization modes will increase. However, the rate of increase of the x-polarization mode is higher compared to the y-polarization mode, as shown in Fig. 5 (a). Therefore, the birefringence will first decrease and then increase with increasing thickness (demarcation is 104 nm). In our experiment (Sec. 3.3), a three-layer (PAH-PSS-PAH) polyelectrolyte coating has an estimated thickness within 15 nm [18], which is under 104 nm. Thus the birefringence always decreases. When the exposed side is filled with a bulk RI liquid, it can be considered that the "thickness" is much higher than 104 nm, thus the birefringence increases with increasing bulk refractive index, as was shown in Fig. 4 (a). Further, the birefringence of the ECF coated with thin-films in different external bulk RI is shown in Fig. 5 (b). The birefringence still increases with respect to the external bulk RI for the same thin-film thickness. Compared with Fig. 4 (a), it can be seen that with or without a thin-film, the birefringence will always increase with respect to the external bulk RI.

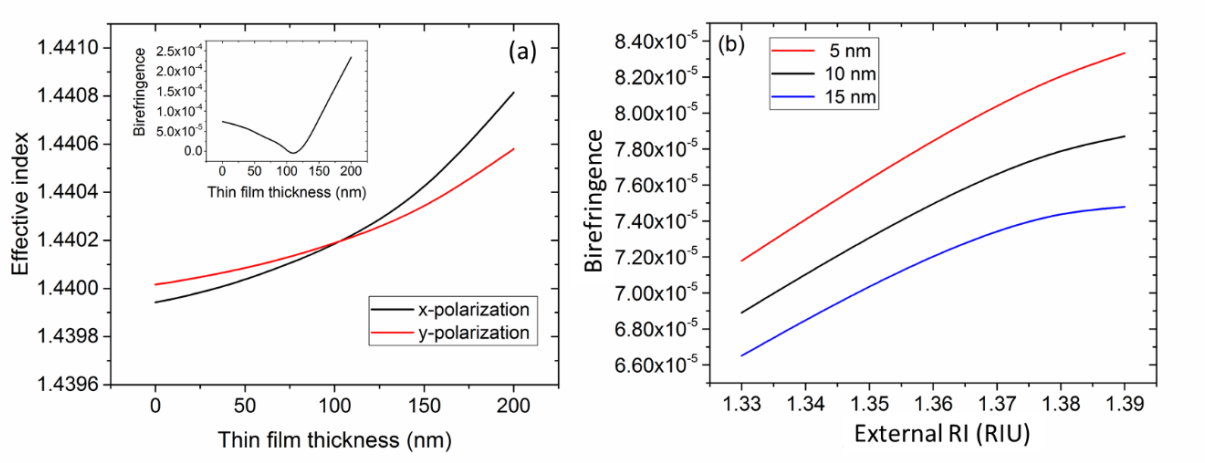

Fig. 5 (a) Numerically modelled values for the effective index of the ECF with different polymer film thicknesses. Inset shows the corresponding birefringence. (b) The birefringence of the ECF with different external bulk RI when the polymer film is 5 nm, 10 nm and 15 nm.

3. Experimental results

3.1 Transmission spectrum of the sensor

A section of the ECF was first cleaved (Photon Kinetics FK11-STD) with a cleaving angle of less than 2.0°, as this is critical for good splicing. Each end of the ECF was then spliced to two single mode fibers (SMF28) using an arc splicer (Fujikura FSM-100P) with settings previously described in detail in [27]. Finally, the structure was connected with a coupler to form a Sagnac loop. Light from a broad-band light source (NKT Photonics SuperK Extreme) was split into clockwise and counterclockwise beams via a 3 dB coupler as it entered the loop. Interference spectra were then measured using an optical spectrum analyzer (OSA, Ando-6315E) with a resolution of 0.05 nm. Different extinction ratios were obtained by adjusting the polarization controller (PC), and the highest extinction ratio achieved was 20 dB, as shown in Fig. 6. The transmission spectra of the Sagnac interferometer with different ECF lengths are also shown in Fig. 6. When the ECF length was 20 cm (Fig. 6(a)), the corresponding free spectral range (FSR) was relatively wide at 230 nm. When the ECF length was increased, the FSR became narrower, such as 145 nm for a 35 cm length (Fig. 6(b)). It is worth mentioning that the spectra contain a higher frequency component that appears to be noise, but is actually the result of interference with higher order modes [19]. This does not adversely affect our sensor as it can be easily filtered out using Fourier techniques (see below).

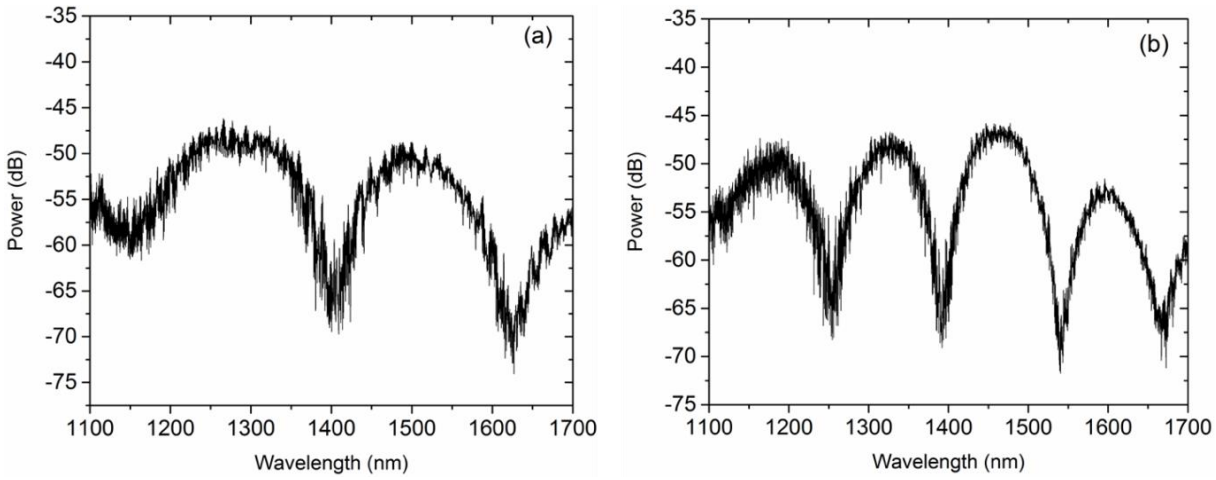

Fig. 6 Sagnac interference spectra with different ECF lengths in air. (a) 20 cm, (b) 35 cm.

3.2 Refractive index sensing

To demonstrate refractive index sensing, the SMF-ECF-SMF structure was inserted into a rigid flow cell (inner diameter of approximately 650 μm), which was then filled with different RI solutions using a pump (LongerPump BT100-1F), as shown in Fig. 1. All experiments were performed in a temperature controlled lab and the flow cell was fixed onto an optical table to avoid any influence of temperature or strain. The spectral response of the sensor to bulk RI by immersing the ECF into different concentrations of sodium chloride in deionized water solutions was measured (Fig. 7 (a)). The length of ECF was 20 cm, which produced two transmission dips over the measured bandwidth of 200 nm. Since the Sagnac interference spectrum is a periodical waveform, it corresponds to a frequency in the spatial frequency domain obtained by applying a fast Fourier transform (FFT) to the wavelength spectrum [28, 29]. Fig. 7 (b) is the FFT spectrum of the first interference spectrum in Fig. 7 (a). The main peak in the FFT spectrum corresponds to the Sagnac interference while other lower peaks at higher frequencies represents effects such as multimode interference and noise. An analysis after FFT filtering reveals more detailed information, as shown in Fig. 7 (c).

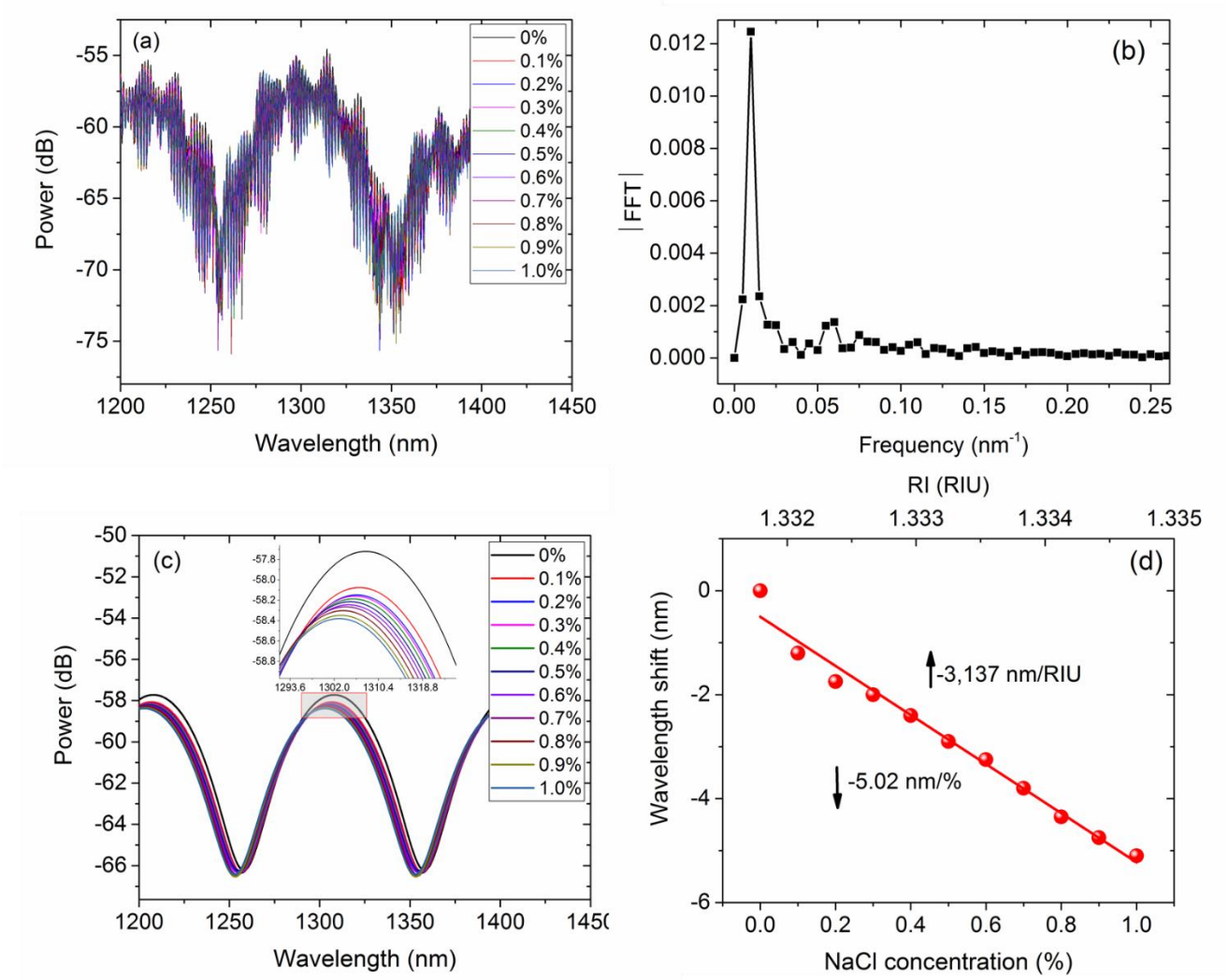

Fig. 7. (a) Spectra of the proposed platform subjected to different external bulk RI. (b) FFT spectrum of the first interference spectrum in Fig. 7 (a). FFT-filtered spectra (c) and wavelength shifts (d) for different concentrations of NaCl.

The wavelength shift was determined from the measured spectra by using the phase change ($\Delta\psi$) information, which was extracted through phase changes associated with the FFT peak [30]. The wavelength shift is then shown in Fig. 7(d) by using the expression $\Delta\lambda=(FSR/2\pi)\Delta\psi$, where FSR is the free spectral range. This technique is advantageous compared to peak tracking a single fringe as it effectively makes use

of the entire spectral data and thus is less susceptible to noise. Converting to RI [31], the sensitivity is estimated to be -3,137 nm/RIU, which has a small difference with the theoretical value of -2,592 nm/RIU. The difference can be attributed to compounded errors associated with light source spectral stability, spectrum analyzer measurements, recording and importing the SEM image for the simulation, and NaCl concentrations.

3.3 Biotin immobilization and streptavidin detection

A new sensor was fabricated in order to demonstrate label-free sensing of biological molecules via the detection of streptavidin using biotin as the capturing probe. The biotin molecules were immobilized onto the exposed-core fiber surface to serve as the capturing probe for streptavidin, the target molecules. The surface-functionalization using biotin, the bio recognition molecules, was carried out using the fuzzy nanoassembly technique [32], which has been used in our previous work [19]. The steps are shown in Fig. 8. First, positively charged poly (allylamine) hydrochloride (PAH, average molecular weight of 15 kDa, 2 mg/mL in 1 M NaCl solution, Sigma Aldrich) and negatively charged poly (sodium 4-styrene sulfonate) (PSS, average molecular weight of 70 kDa, 2 mg/mL in 1 M NaCl solution, Sigma Aldrich) were deposited on the exposed core fiber using the layer by layer deposition technique. Between each layer the sensor was rinsed with 1 M NaCl solution to remove unattached PAH and PSS. The last PAH layer provides amino groups for the immobilization of biotin (Ez-Link Sulfo-NHS-Biotin, 0.5 mg/ml in phosphate buffer solution, Thermo Fisher), which were freshly prepared in phosphate buffer solution (PBS buffer, standard 1X, pH = 7.4, Sigma Aldrich). The sensor was then rinsed by PBS to remove the unbound biotin, completing the surface-functionalization. The steps of streptavidin detection are shown in Fig. 8 (b). First, a solution of streptavidin in PBS (Thermo Fisher, 0.2 mg/ml in PBS) was freshly prepared and passed through the flow cell. The sensor was then rinsed with PBS to remove the unbound streptavidin.

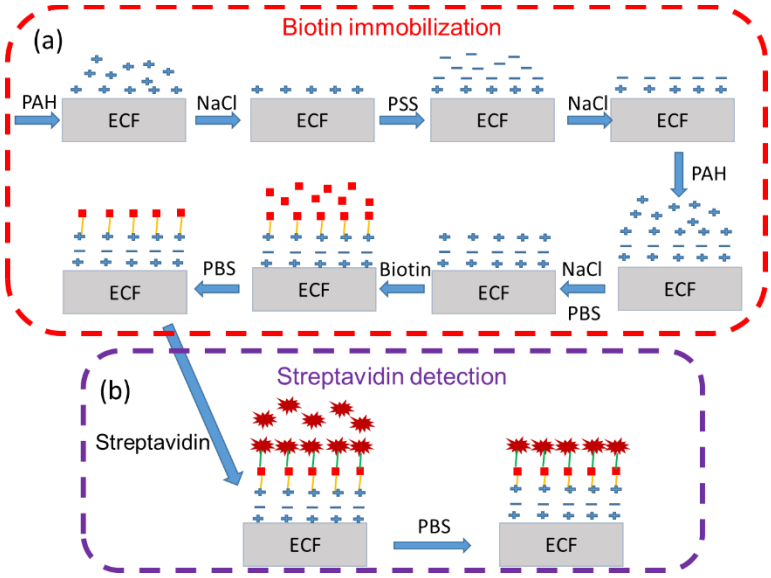

Fig. 8 Detailed procedures of the (a) surface-functionalization and (b) bio-sensing.

The FFT-filtered Sagnac interference spectra measured while different solutions were passed through the flow cell are shown in Fig. 9 (a). Note that the FSR of the sensor used in this experiment (Fig. 9(a)) is slightly different to that used for the refractive index sensing experiments (Fig. 7(a)) due to slightly different lengths of ECF used, L = 15 cm and L = 20 cm, respectively. However, this has little impact on the sensor accuracy as the FFT phase-tracking technique we have used has little dependence on noise and the FSR. To confirm that PAH and PSS were correctly attached to the surface of the ECF, the ECF was first deposited with the PAH-PSS-PAH-PSS-PAH layered configuration. In the subsequent experiments, we can know whether the PAH and PSS were correctly attached by tracking the spectrum change.

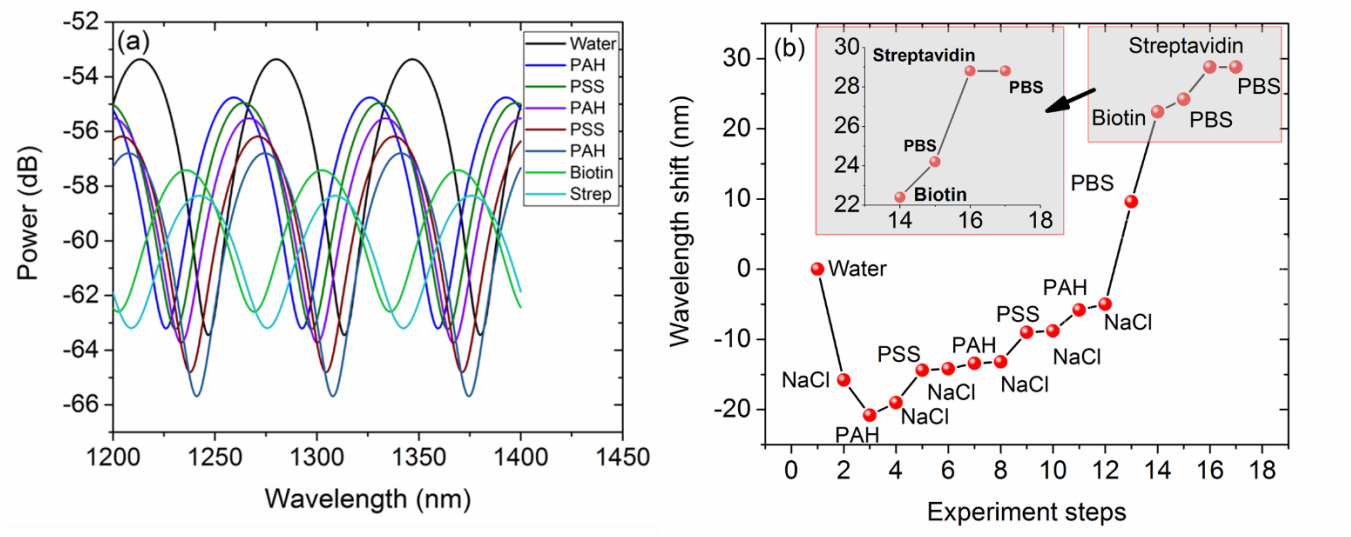

Fig. 9 (a) Filtered spectra of the proposed sensor corresponding to different coating steps and (b) the wavelength shift with each experiment step.

The filtered spectra of the proposed sensor to different solutions, and thus different thin-film deposition steps, are shown in Fig. 9. Starting from water, the transmission spectrum in this case was selected as a reference spectrum. Next, the sensor was rinsed extensively with 1 M NaCl solution, whose bulk RI is higher than water, which leads to a shift to shorter wavelengths, as expected (see Fig. 4). PAH was then filled into the flow cell and flowed through the sensor. The bulk RI of PAH solution is higher than that of the 1M NaCl solution and the polymer film did not have sufficient localized RI change to counter the difference in bulk RI of the NaCl compared to the PAH solution, so the spectrum still shifted to shorter wavelengths. After rinsing with 1 M NaCl solution, the polymer film formed completely, and led to a birefringence decrease and wavelength increase. The thickness of the polymer film increases with the deposition of alternating layers of PAH and PSS leading to further shifts to longer wavelengths. The sensor was then rinsed with PBS as it is used as a standard biological buffer for biotin and streptavidin in our experiment. Because the bulk RI of PBS is lower than that of the 1M NaCl solution, while the thickness of the polymer film did not change, the birefringence of the ECF decreased, leading to a shift of the Sagnac spectrum to longer wavelengths.

Afterwards, the NHS-Biotin solution was flown through the sensor. Biotin was immobilized on the sensor surface as the capturing probe, and the thickness of the thin-film increased leading to a shift of the Sagnac interference spectrum to longer wavelengths. Then, the sensor was exposed to a buffer solution containing streptavidin as the target molecules. The thickness of the thin-film increased when streptavidin was bound to the biotin immobilized on the sensor surface. Thus, a shift to longer wavelengths was recorded. The wavelength shift of the sensor in response to streptavidin binding was 5 nm, which is smaller than the response to biotin (12 nm). This is consistent with previously published evanescent field based sensing [19] and is attributed to a combination of higher binding density of biotin and that biotin binds relatively closer to the optical fiber surface. Closer molecules will have exponentially stronger interaction with the evanescent field, and thus induce a larger wavelength shift.

To confirm the binding between biotin and streptavidin, a control sensor in which the biotin immobilization step was omitted was subjected to the same streptavidin solution. It can be seen from Fig. 10 (a) that the wavelength shifts are similar to Fig. 9 (b) before the sensor was flown through with the biotin solution. However, when the sensor was exposed to the streptavidin solution, there was only a small wavelength change, caused by the different bulk RI of the PBS solution and the streptavidin solution. A comparison of the results is shown in Fig. 10 (b). The results confirm that the wavelength shift of streptavidin in Fig. 9 is due to the presence of the capturing probe biotin rather than bulk RI difference between PBS solution and streptavidin, or spurious effects such as non-specific adsorption of streptavidin to the polyelectrolyte surface.

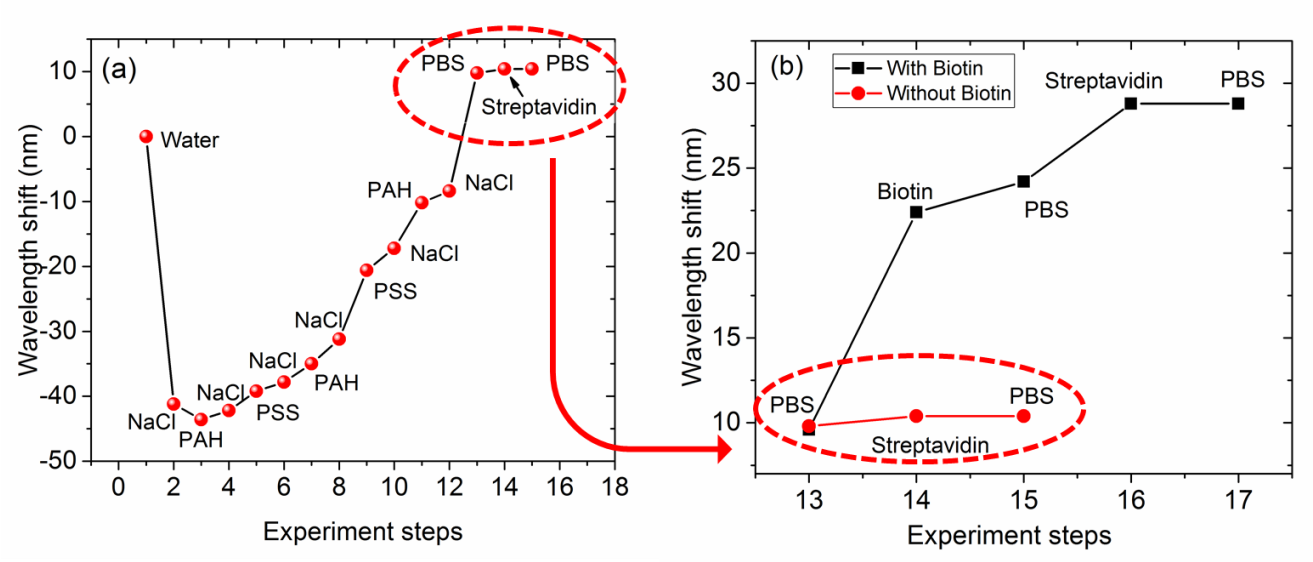

Fig. 10 (a) The wavelength shift for each experiment step and (b) the wavelength shift when streptavidin in PBS buffer was flown through the sensor with (black) and without (red) biotin.

4. Conclusion

A novel, high sensitivity Sagnac-interferometer biosensor based on exposed-core microstructured optical fiber (ECF) has been designed and implemented. The proposed sensor has a high bulk refractive index sensitivity up to -3,137 nm/RIU and its use as a label-free biosensor has been demonstrated. While biotin and streptavidin were used in our work as the probe-target pair as a biosensor demonstration, the sensor can equally be used with other biological capturing probes for a variety of target molecules. As an optical fiber based platform, it has advantages of bio-compatibility, small size, high stability and low cost, yet is robust and simple to fabricate compared to other similar techniques, such as the use of tapered micro-fibers.

Acknowledgements

Stephen C. Warren-Smith is funded by a Ramsay Fellowship provided by the University of Adelaide. This work was performed, in part, at the Optofab node of the Australian National Fabrication Facility, a company established under the National Collaborative Research Infrastructure Strategy to provide nano and micro-fabrication facilities for Australia's researchers. Xuegang Li gratefully acknowledges financial support from the China Scholarship Council. This work was supported in part by the Fundamental Research Funds for the Central Universities under Grant N160406004. Linh Viet Nguyen acknowledges the support of the Australian Government's Cooperative Research Centres Program. The authors acknowledge Peter Henry and Alastair Dowler for their contribution to the fiber fabrication.

References

[1] J.-h. Liou, and C.-p. Yu, "All-fiber Mach-Zehnder interferometer based on two liquid infiltrations in a photonic crystal fiber," *Optics Express,* vol. 23, no. 5, pp. 6946-6951, 2015.

[2] X. W. Tang, S. Bansaruntip, N. Nakayama, E. Yenilmez, Y. L. Chang, and Q. Wang, "Carbon nanotube DNA sensor and sensing mechanism," *Nano Letters,* vol. 6, no. 8, pp. 1632-1636, Aug 9, 2006.

[3] Y. Zhao, X. G. Li, L. Cai, and Y. Yang, "Refractive index sensing based on photonic crystal fiber interferometer structure with up-tapered joints," *Sensors and Actuators B-Chemical,* vol. 221, pp. 406-410, Dec 31, 2015.

[4] Y. Q. Wu, D. Y. Zhang, P. Yin, and F. Vollmer, "Ultraspecific and highly sensitive nucleic acid detection by integrating a DNA catalytic network with a label-free microcavity," *Small,* vol. 10, no. 10, pp. 2067-2076, May 28, 2014.

[5] J. D. Suter, I. M. White, H. Y. Zhu, H. D. Shi, C. W. Caldwell, and X. D. Fan, "Label-free quantitative DNA detection

using the liquid core optical ring resonator," *Biosensors & Bioelectronics,* vol. 23, no. 7, pp. 1003-1009, Feb 28, 2008.

[6] S. Y. Niu, Q. Y. Li, R. Ren, and S. S. Zhang, "Enzyme-enhanced fluorescence detection of DNA on etched optical fibers," *Biosensors & Bioelectronics,* vol. 24, no. 9, pp. 2943-2946, May 15, 2009.

[7] X. J. Liu, and W. H. Tan, "A fiber-optic evanescent wave DNA biosensor based on novel molecular beacons," *Analytical Chemistry,* vol. 71, no. 22, pp. 5054-5059, Nov 15, 1999.

[8] E. Heydari, J. Buller, E. Wischerhoff, A. Laschewsky, S. Doring, and J. Stumpe, "Label-free biosensor based on an all-polymer DFB laser," *Advanced Optical Materials,* vol. 2, no. 2, pp. 137-141, Feb, 2014.

[9] A. Bertucci, A. Manicardi, A. Candiani, S. Giannetti, A. Cucinotta, G. Spoto, M. Konstantaki, S. Pissadakis, S. Selleri, and R. Corradini, "Detection of unamplified genomic DNA by a PNA-based microstructured optical fiber (MOF) Bragg-grating optofluidic system," *Biosensors & Bioelectronics,* vol. 63, pp. 248-254, Jan 15, 2015.

[10] X. Fang, C. R. Liao, and D. N. Wang, "Femtosecond laser fabricated fiber Bragg grating in microfiber for refractive index sensing," *Optics Letters,* vol. 35, no. 7, pp. 1007-1009, Apr 1, 2010.

[11] Y. Ma, X. G. Qiao, T. Guo, R. H. Wang, J. Zhang, Y. Y. Weng, Q. Z. Rong, M. L. Hu, and Z. Y. Feng, "Reflective fiber-optic refractometer based on a thin-core fiber tailored Bragg grating reflection," *Optics Letters,* vol. 37, no. 3, pp. 323-325, Feb 1, 2012.

[12] H. M. R. Goncalves, L. Moreira, L. Pereira, P. Jorge, C. Gouveia, P. Martins-Lopes, and J. R. A. Fernandes, "Biosensor for label-free DNA quantification based on functionalized LPGs," *Biosensors & Bioelectronics,* vol. 84, pp. 30-36, Oct 15, 2016.

[13] M. Han, F. W. Guo, and Y. F. Lu, "Optical fiber refractometer based on cladding-mode Bragg grating," *Optics Letters,* vol. 35, no. 3, pp. 399-401, Feb 1, 2010.

[14] D. J. J. Hu, J. L. Lim, M. Jiang, Y. X. Wang, F. Luan, P. P. Shum, H. F. Wei, and W. J. Tong, "Long period grating cascaded to photonic crystal fiber modal interferometer for simultaneous measurement of temperature and refractive index," *Optics Letters,* vol. 37, no. 12, pp. 2283-2285, Jun 15, 2012.

[15] Z. Y. Wang, J. R. Heflin, K. Van Cott, R. H. Stolen, S. Ramachandran, and S. Ghalmi, "Biosensors employing ionic self-assembled multilayers adsorbed on long-period fiber gratings," *Sensors and Actuators B-Chemical,* vol. 139, no. 2, pp. 618-623, Jun 4, 2009.

[16] S. Lepinay, A. Staff, A. Ianoul, and J. Albert, "Improved detection limits of protein optical fiber biosensors coated with gold nanoparticles," *Biosensors & Bioelectronics,* vol. 52, pp. 337-344, Feb 15, 2014.

[17] M. C. Hsieh, Y. H. Chiu, S. F. Lin, J. Y. Chang, C. O. Chang, and H. K. Chiang, "Amplification of the signal intensity of fluorescence-based fiber-optic biosensors using a fabry-perot resonator structure," *Sensors,* vol. 15, no. 2, pp. 3565-3574, Feb, 2015.

[18] Y. Zhang, H. Shibru, K. L. Cooper, and A. B. Wang, "Miniature fiber-optic multicavity fabry-perot interferometric biosensor," *Optics Letters,* vol. 30, no. 9, pp. 1021-1023, May 1, 2005.

[19] L. V. Nguyen, K. Hill, S. Warren-Smith, and T. Monro, "Interferometric-type optical biosensor based on exposed core microstructured optical fiber," *Sensors and Actuators B-Chemical,* vol. 221, pp. 320-327, Dec 31, 2015.

[20] W. J. Yu, T. T. Lang, J. C. Bian, and W. Kong, "Label-free fiber optic biosensor based on thin-core modal interferometer," *Sensors and Actuators B-Chemical,* vol. 228, pp. 322-329, Jun 2, 2016.

[21] S. Gao, L. P. Sun, J. Li, L. Jin, Y. Ran, Y. Y. Huang, and B. O. Guan, "High-sensitivity DNA biosensor based on microfiber Sagnac interferometer," *Optics Express,* vol. 25, no. 12, pp. 13305-13313, Jun 12, 2017.

[22] S. M. Chen, Y. Liu, Q. Liu, and W. Peng, "Temperature-compensating fiber-optic surface plasmon resonance biosensor," *IEEE Photonics Technology Letters,* vol. 28, no. 2, pp. 213-216, Jan 15, 2016.

[23] J. Lu, D. Spasic, F. Delport, T. Van Stappen, I. Detrez, D. Daems, S. Vermeire, A. Gils, and J. Lammertyn, "Immunoassay for detection of infliximab in whole blood using a fiber-optic surface plasmon resonance biosensor," *Analytical Chemistry,* vol. 89, no. 6, pp. 3664-3671, Mar 21, 2017.

[24] J. D. Lu, T. Van Stappen, D. Spasic, F. Delport, S. Vermeire, A. Gils, and J. Lammertyn, "Fiber optic-SPR platform for fast and sensitive infliximab detection in serum of inflammatory bowel disease patients," *Biosensors & Bioelectronics,* vol. 79, pp. 173-179, May 15, 2016.

[25] S. Sharma, S. P. Usha, A. M. Shrivastav, and B. D. Gupta, "A novel method of SPR based SnO_2: GNP nano-hybrid decorated optical fiber platform for hexachlorobenzene sensing," *Sensors and Actuators B-Chemical,* vol. 246, pp. 927-936, Jul, 2017.

[26] C. Y. Han, H. Ding, X. L. Li, and S. F. Dong, "Temperature insensitive refractive index sensor based on single-mode micro-fiber Sagnac loop interferometer," *Applied Physics Letters,* vol. 104, no. 18, May 5, 2014.

[27] S. C. Warren-Smith, R. Kostecki, L. V. Nguyen, and T. M. Monro, "Fabrication, splicing, Bragg grating writing, and polyelectrolyte functionalization of exposed-core microstructured optical fibers," *Optics Express,* vol. 22, no. 24, pp. 29493-29504, Dec 1, 2014.

[28] L. V. Nguyen, S. C. Warren-Smith, H. Ebendorff-Heidepriem, and T. M. Monro, "Interferometric high temperature sensor using suspended-core optical fibers," *Optics Express,* vol. 24, no. 8, pp. 8967-8977, Apr 18, 2016.

[29] J. H. Liou, and C. P. Yu, "All-fiber Mach-Zehnder interferometer based on two liquid infiltrations in a photonic crystal

fiber," *Optics Express,* vol. 23, no. 5, pp. 6946-6951, Mar 9, 2015.
[30] J.W. Silverstone, S. McFarlane, C.P.K. Manchee, and A. Meldrum, "Ultimate resolution for refractometric sensing with whispering gallery mode microcavities," Optics Express, vol. 20, no. 8, pp. 8284-8295, Mar 4, 2012.
[31] W. Haynes, "Concentrative properties of aqueous solutions: Density, refractive index, freezing point depression, and viscosity," *CRC Handbook of chemistry and physics, 92nd edn, Internet Version, CRC Press/Taylor and Francis, Boca Raton*, 2012.
[32] G. Decher, "Fuzzy nanoassemblies: Toward layered polymeric multicomposites," *Science,* vol. 277, no. 5330, pp. 1232-1237, Aug 29, 1997.

Biographies

Xue-gang Li was born in Hebei, China, in December 1991. He received his B.A. from the College of Information Science and Engineering from the Northeastern University, China, in 2014. He is now a visiting PhD student of the University of Adelaide. His research interests are photonic crystal fiber sensors, optical modal interference sensors, in-fiber interferometer and its sensing applications. He has authored and co-authored more than ten scientific papers.

Linh V. Nguyen was born in Hanoi, Vietnam. After graduating with a BSc. degree in Applied Physics from Hanoi University of Science in 2002 he moved to South Korea and earned a PhD in Information and Communications from Gwangju Institute of Science and Technology (GIST), South Korea, in 2009. His graduate works focused on the development of fiber-optics devices for applications in fiber sensing, fiber lasers and all-optical signal processing. In early 2010 he moved to Edith Cowan University (ECU) in Western Australia to work on the development of fiber-optic sensors for applications in desalination and seawater-related industries. His experiences range from fabrication (MCVD, DT) and characterization of specialty optical fiber to development of fiber devices (e.g. gratings, sensors, lasers, micro-machined fiber). In 2011 he joined the Institute for Photonics & Advanced Sensing (IPAS), School of Physical Sciences at the University of Adelaide in 2011, first as an Australian Research Council (ARC) Super Science Fellow leading a project toward development of rapid protein sensing and blood typing platform at crime scenes, and subsequently as a Research Associate on a project toward the development of tools for in-field surveillance of pathogens.

Yong Zhao received his M.A. and Ph.D. degrees, respectively, in precision instrument & automatic measurement with laser and fiber-optic techniques from the Harbin Institute of Technology, China, in 1998 and 2001. He was awarded a first prize scholarship in 2000 by the China Instrument and Control Society and the Sintered Metal Corporation (SMC) scholarship in Japan. He was a postdoctoral fellow in the Department of Electronic Engineering of Tsinghua University from 2001 to 2003, and then worked as an associate professor in the Department of Automation, Tsinghua University of China. In 2006, he was a visiting scholar of University of Illinois in Urbana and Champagne, USA. In 2008, he was awarded as the "New Century Excellent Talents in University" by the Ministry of Education of China. In 2009, he was awarded as the "Liaoning Bai-Qian-Wan Talents" by Liaoning Province. In 2011, he was awarded by the Royal Academy of Engineering as an academic research fellow of City University London. In 2014, he was awarded by the National Science Foundation for Distinguished Young Scholars of China. In 2015, he was honored as the Yangtze River Scholar Distinguished Professor by the Ministry of Education of China. Now he is working in Northeastern University as a full professor. As the academic leader and director of his research institute, his current research interests are the development of fiber-optic sensors and devices, fiber Bragg grating sensors, novel sensor materials and principles, slow light and sensor technology and optical measurement technologies. He has authored and co-authored more than 260 scientific papers and conference presentations, 23 patents, and 5 books. He is a member in the Editorial Boards of the international journals of Sensor Letters, Instrumentation Science & Technology, Journal of Sensor Technology, and Advances in Optical

Technologies.

Stephen C. Warren-Smith completed his PhD in 2011 at the University of Adelaide, Australia, on the topic of microstructured optical fiber chemical sensing. He was then employed from 2011 to 2014 as an Australian Research Council (ARC) Super Science Fellow at the Institute for Photonics and Advanced Sensing and the School of Chemistry and Physics at the University of Adelaide, working on optical fiber biosensing for women's health applications. In 2015 and 2016 he worked as a European Union Marie Curie International Incoming Fellow at the Institute of Photonic Technology, Jena, Germany, on a project investigating the micro/nano-structuring of optical fibers for sensing. Since October 2016 he is with the University of Adelaide as a Ramsay Fellow.

Heike Ebendorff-Heidepriem obtained her PhD in chemistry from the University of Jena, Germany in 1994 and subsequently held two prestigious fellowships. From 2001-2004 she was with the Optoelectronics Research Centre at the University of Southampton, UK. Heike came to the University of Adelaide in 2005. She was awarded the Woldemar A. Weyl International Glass Science Award in 2001, the International Zwick Science Award in 2009 and the University of Adelaide Women's Research Excellence Mid-Career Award in 2014. Heike has published over 230 refereed journal papers and conference proceedings, including 5 review papers and 9 post-deadline papers, and raised approximately $12M for research. Heike's research focuses on the development of novel optical glasses, fibres, surface functionalization and sensing approaches.